

# STA-Unet: Rethink the semantic redundant for Medical Imaging Segmentation

Vamsi Krishna Vasa  
Arizona State University  
vvasa1@asu.edu

Wenhui Zhu  
Arizona State University  
wzhu59@asu.edu

Xiwen Chen  
Clemson University  
xiwenc@g.clemson.edu

Peijie Qiu  
Washington University in St.Louis  
peijie.qiu@wustl.edu

Xuanzhao Dong  
Arizona State University  
xdong64@asu.edu

Yalin Wang  
Arizona State University  
ylwang@asu.edu

## Abstract

*In recent years, significant progress has been made in the medical image analysis domain using convolutional neural networks (CNNs). In particular, deep neural networks based on a U-shaped architecture (UNet) with skip connections have been adopted for several medical imaging tasks, including organ segmentation. Despite their great success, CNNs are not good at learning global or semantic features. Especially ones that require human-like reasoning to understand the context. Many UNet architectures attempted to adjust with the introduction of Transformer-based self-attention mechanisms, and notable gains in performance have been noted. However, the transformers are inherently flawed with redundancy to learn at shallow layers, which often leads to an increase in the computation of attention from the nearby pixels offering limited information. The recently introduced Super Token Attention (STA) mechanism adapts the concept of superpixels from pixel space to token space, using super tokens as compact visual representations. This approach tackles the redundancy by learning efficient global representations in vision transformers, especially for the shallow layers. In this work, we introduce the STA module in the UNet architecture (STA-Unet), to limit redundancy without losing rich information. Experimental results on four publicly available datasets demonstrate the superiority of STA-Unet over existing state-of-the-art architectures in terms of Dice score and IOU for organ segmentation tasks. The code is available at <https://github.com/Retinal-Research/STA-UNet>.*

## 1. Introduction

Leveraging advancements in deep learning, computer vision techniques have become integral to medical image analysis. Among these techniques, image segmentation holds significant importance. Specifically, precise and re-

liable segmentation of medical images is crucial, serving as a foundational component in computer-aided diagnosis and image-guided surgical procedures [5, 10].

Current approaches to medical image segmentation predominantly utilize fully convolutional neural networks (FCNNs) with a U-shaped architecture [16, 18, 30]. The widely recognized U-Net [30], a classic example of this architecture, features a symmetric Encoder-Decoder design linked by skip connections. The encoder extracts deep features with extensive receptive fields through multiple convolutional and down-sampling layers. The decoder then up-samples these deep features back to the original resolution for precise pixel-level semantic predictions, while the skip connections merge high-resolution features from various scales within the encoder to mitigate spatial information loss due to down-sampling. This well-crafted design has enabled U-Net to succeed significantly across numerous medical imaging tasks. The remarkable performance of these FCNN-based methods in cardiac segmentation, organ delineation, and lesion detection underscores CNNs' robust capability in learning distinguishing features.

While CNN-based techniques have demonstrated impressive results in medical image segmentation, they still fall short of the high accuracy standards required for clinical applications. Medical image segmentation remains a challenging problem, primarily due to the convolution operation's inherent focus on local features, making it difficult for CNNs to capture explicit global and long-range semantic interactions. Recently, inspired by the success of Transformers in natural language processing (NLP) [34], researchers have started to explore their application in the vision domain [4, 8, 27] to address the limitations of CNNs using self-attention. While the Vision Transformer (ViT) excels at capturing long-range dependencies across image patches with its large receptive field, it faces challenges in retaining fine-grained local context due to its lack of inherent locality.

To address this issue, recent approaches [3,5,11,38] have proposed hybrid models that combine CNNs and ViTs in UNet architectures. However, these models significantly increase computational complexity and the number of parameters. Over-parameterization is a prevalent problem in deep learning, frequently resulting in feature redundancy and suboptimal feature representation [6,23,24]. Despite its impact, the existing research has not thoroughly explored or considered this challenge. In addition to the methods discussed, several approaches aim to enhance the architectural design of UNet. For instance, Att-UNet [28] introduces attention-based skip connections to filter out irrelevant features, while UNet++ [39] replaces traditional skip connections, such as concatenation or addition, with nested dense skip pathways. UCTransNet [35] provides an in-depth analysis of various skip connection strategies and proposes using a channel transformer as an alternative to conventional skip connections. Recently proposed Seg-Swinunet [40] leverages the feature map with the highest semantic content (i.e., the decoder’s final layer) to provide additional supervision to other blocks, reducing feature redundancy through feature distillation. However, we investigate this redundancy from a different perspective.

Our preliminary analysis indicates a significant similarity among blocks in the shallow layers of Transformer UNet architectures [3,5,11,38]. This observation implies that the model exhibits a form of inertia learning pattern in the shallow layers, leading to a failure to effectively capture and encode complex contextual information. Existing research has seldom addressed this inherent limitation. [15] adapt the concept of superpixels from the pixel domain to the token domain, considering super tokens as a concise representation of visual information. This approach integrates sparse association learning, self-attention, and token space mapping to enhance visual token processing efficiency, leading to rich feature learning. In this study, we attempted to tackle redundancy by integrating Super Token Attention in UNet architecture and enhancing the performance of the multi-organ segmentation challenge.

The main contributions of our work are three-fold: (i) We highlight the redundancy in the shallow layers of the transformer-based UNets to promote research in this area. (ii) We integrate the Super Token Attention (STA) block into the UNet architecture to minimize the redundancy observed in other Transformer-based UNet models while preserving the rich semantic information necessary for effective learning. (iii) Our comprehensive evaluation across four publicly available medical imaging datasets demonstrated the superiority of the proposed method over existing relevant SOTA methods in organ segmentation tasks.

## 2. Related Work

**UNet-based architectures:** Early methods for medical image segmentation primarily relied on contour-based approaches and traditional machine learning techniques [12,33]. However, the advent of deep convolutional neural networks (CNNs) brought significant advancements, with the introduction of Unet [30] specifically designed for medical image segmentation. The U-Net’s distinctive U-shaped architecture, noted for its simplicity and exceptional performance, has inspired numerous variations, including Res-Unet [37], Dense-Unet [25], U-Net++ [39], and UNet3+ [14]. CNN-based architectures are flawed in capturing redundant information and do not focus on learning the dependencies between different regions of the canvas.

**Transformer based UNet architectures :** Vaswani et al. [34] introduced the Self-attention mechanism using Transformers in Natural Language Processing to weigh the importance of different words relative to each other. This advancement led to the development of the Vision Transformers (ViT) [8,27], which adapts the transformer architecture to achieve comparable success in image processing tasks. These transformers are integrated with the UNet designs [3,5,38], with the aim to combine the strengths of CNNs and Transformers.

Chen et al. [5] attempted to combine the Transformers in the encoder and decoder of the UNet architecture. The Transformer block in the encoder tokenizes image patches from a CNN feature map to capture global context. Meanwhile, the decoder upsamples these encoded features and merges them with high-resolution feature maps from the CNN. Although the ViT excels in capturing long-range dependencies between image patches (tokens) due to its large receptive field, it faces challenges in maintaining detailed local context because of its lack of inherent locality. To overcome this limitation, Swin-Unet [3] adapts the attention mechanism using shifting window tokens [27]. This allows the model to restrict window-based attention to local regions. Although this adaptation limits the redundancy, it is not completely eradicated from the shallow layers. Meanwhile, Zhu et al. [40] proposed Seg-SwinUNet, which addresses performance issues in UNet for medical image segmentation by balancing supervision between the encoder and decoder and reducing feature redundancy. It tried to enhance UNet by using feature distillation to provide additional supervision from the most semantically rich feature map, improving segmentation accuracy with minimal computational overhead. However, the work is still limited to Swin-UNet, and no further study has been conducted to incorporate this approach with other architectures.

Xu et al. [38] proposed LeViT-UNet, where LeViT [9] as the encoder within the LeViT-UNet framework, as it effectively balances accuracy and efficiency in Transformer blocks. Additionally, skip connections integrate multi-scale

feature maps derived from the Transformer and convolutional blocks of LeViT into the decoder. As the LeViT plays the central role in preserving and passing information to the decoder, the redundant token information couldn't be avoided, Leading to increased computational cost. Recently proposed HiFormer [11] integrates CNN and transformer architectures to capture both local and global features for medical image segmentation. It employs multi-scale feature representations using a Swin Transformer and CNN-based encoder, combined through a Double-Level Fusion (DLF) module in the encoder-decoder structure. Extensive experiments show HiFormer's superior performance in accuracy and efficiency compared to other methods.

**Mitigating feature redundancy:** Oktay et al. [28] proposed Attention Gates (AG) to focus on target structures of varying shapes and sizes by suppressing irrelevant regions and highlighting important features. This eliminates the need for external localization modules, as AGs can be easily integrated into CNN architectures like U-Net with minimal computational cost. Zhou et al. [39] proposed UNet++ architecture to deeply supervise the encoder-decoder network that connects the encoder and decoder through nested, dense skip pathways. These redesigned pathways aim to reduce the semantic gap between the encoder's and decoder's feature maps, making the learning task easier for the optimizer. Wang et al. [35] proposed UC-TransNet replaces traditional U-Net skip connections with the Channel Transformer (CTrans) module, which includes two sub-modules: the Channel Cross fusion with Transformer (CCT) for multi-scale channel fusion and Channel-wise Cross-Attention (CCA) to guide fused features into the decoder. This new connection structure addresses semantic gaps between encoder and decoder features for improved segmentation. Zhu et al. [40] proposed model balances supervision between the encoder and decoder and reduces feature redundancy in UNet by providing additional supervision from the most semantically rich feature map (the last layer of the decoder) to other blocks. It leverages feature distillation to minimize redundant information and enhance learning efficiency. This method integrates seamlessly into existing UNet architectures with minimal computational overhead, improving performance across various medical image segmentation tasks.

### 3. Preliminary Analysis

Here, we employ Centered Kernel Alignment (CKA) [19] to investigate the recent popular U-net models, including SwinUnet, LeViT-Unet, TransUnet, and HiFormer. This technique allows us to compute the block-wise similarity even when the layers' sizes are different. The block-wise similarity matrices are able to offer insights into how different neural network architectures learn and represent information at various layers (or blocks) throughout the training

process.

Mathematically, given two sets of representations  $\mathbf{X}$  and  $\mathbf{Y}$ , we first compute their gram matrices  $\mathbf{K}$ ,  $\mathbf{L}$  via the Radial Basis Function (RBF),

$$\begin{aligned} \mathbf{K}_{ij} &= \exp(-\|\mathbf{X}_i - \mathbf{X}_j\|^2), \\ \mathbf{L}_{ij} &= \exp(-\|\mathbf{Y}_i - \mathbf{Y}_j\|^2), \end{aligned} \quad (1)$$

where  $\mathbf{K}_{ij}$  and  $\mathbf{L}_{ij}$  denotes the  $i$ th row and  $j$ th column element.  $\mathbf{X}_i, \mathbf{X}_j, \mathbf{Y}_i - \mathbf{Y}_j$  denotes the  $i$ th and  $j$ th sample of the set  $\mathbf{X}, \mathbf{Y}$ , respectively. Afterward, the similarity matrix is computed through RBF-CKA as,

$$RBF - CKA = \frac{\text{tr}(\mathbf{KHLH})}{\sqrt{\text{tr}(\mathbf{KHKH})\text{tr}(\mathbf{LHLH})}}, \quad (2)$$

where  $\mathbf{H}_n = \mathbf{I}_n - \frac{1}{n}\mathbf{1}\mathbf{1}^\top$  denotes the centering matrix.  $\mathbf{I}_n$  denotes a identity matrix with shape  $n \times n$ , where  $n$  denotes the number of samples in the set.

In Fig. 1, we present the results of our investigation, where high values in off-diagonal elements typically indicate strong similarities between corresponding blocks. Across various architectures, the similarity matrices generally exhibit higher degrees of similarity among blocks in the shallow blocks, suggesting a high level of redundancy in these early layers. This immediately implies that the neural network is lazy at the shallow blocks and fails to learn rich information. This observation motivates our efforts to address and reduce such redundancy in the proposed work.

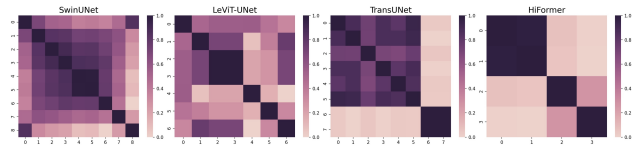


Figure 1. The block-wise similarity calculated by RBF-CKF [19]. The indices are ordered from shallow blocks to deep blocks. For the sake of better visualization, we normalize it to 0~1 by using min-max normalization.

## 4. Method

### 4.1. Super Token Attention Module

Based on the analysis presented in Section 3, there is clear evidence of redundancy in the shallow layers of transformer-based architectures, which results in inefficient information retention. Super tokens [15] can mitigate this flaw by learning efficient global representation. Super tokens are considered as a concise representation of visual information by adapting the concepts of superpixels [17] from pixel domain to token domain. This method combines sparse association learning, self-attention, and token space mapping to improve the efficiency of visual token processing. We re-introduce the Super Token Attention in form of

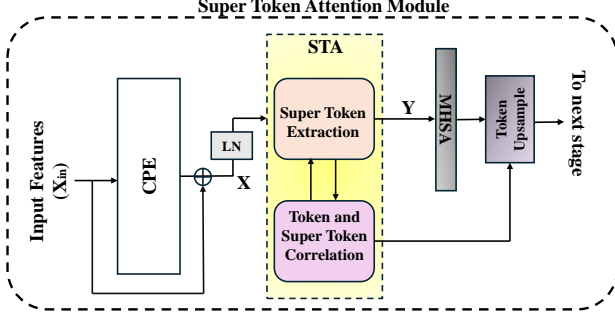


Figure 2. Super Token Attention (STA) Module incorporated in the UNet architecture.

STA Module in the UNet architecture to leverage its benefits for the Medical Image Segmentation task.

Huang et al. achieves Super Token Attention in three stages, Convolutional Position Embedding (CPE), Super Token Attention (STA) and Convolutional Feed-Forward Network (ConvFFN). The CPE stage comprises of the Residual DW layer with  $3 \times 3$  depth-wise convolution over input  $X_{in} \in \mathbb{R}^{H \times W \times C}$ . CPE is more flexible for arbitrary input resolutions as it can learn absolute positions through zero padding, unlike absolute [34] and relative [26, 27] positional encodings. Emphasizing on ConvFFN, which is a collection of convolutional layers with GeLu [13] activation to calculate the learned representation post attention mechanism. The presence of skip connection compensate for this these blocks with no performance degradation, Thus we restrict this stage in our STA-block:

$$\mathbf{X} = \text{CPE}(X_{in}) + X_{in} \quad (3)$$

$$\mathbf{Y} = \text{STA}(\text{LN}(\mathbf{X})) + \mathbf{X} \quad (4)$$

The revised STA Module is illustrated in Fig 2. In STA stage, Super Token Extraction follows k-mean based super-pixel algorithm in Super Sampling Networks [17] to map the pixels to token space. The tokens can be denoted as  $X \in \mathbb{R}^{C \times N}$ .  $N$  is the number of tokens given by  $H \times W$ . Each token (denoted by  $X_i \in \mathbb{R}^{C \times 1}$ ) belongs to one of the Super tokens (denoted by  $S \in \mathbb{R}^{m \times c}$ ).  $m$  is the number of super tokens. If the grid size of  $h \times w$ , number of super tokens  $m$  can be calculated as  $m = \frac{H}{h} \times \frac{W}{w}$ .

Token and Super token correlation aims to calculate the  $X_i$  to  $S_j$  association ( $Q_{ij}$ ) and update the Super tokens. We calculate the  $Q$  using Eq. 5 to attain the the attention type weights.

$$Q = \text{Softmax}\left(\frac{XS}{\sqrt{C}}\right) \quad (5)$$

We limited this to a single iteration based on conclusive experiments and performance analysis. The super token is then updated as weighted sum of tokens defined as:

$$S = (\bar{Q})^T X \quad (6)$$

For reduced computational power, we limit the association calculations to the surrounding nine super tokens. We apply the standard self-attention to the sampled super tokens  $S \in \mathbb{R}^{m \times C}$ :

$$\text{Attn}(S) = \text{Softmax}\left(\frac{q(S)k^T(S)}{\sqrt{C}}\right)v(S) \quad (7)$$

$q(S) = SW_q$ ,  $k(S) = SW_k$ ,  $v(S) = SW_v$ , where  $(W_q, W_k, W_v)$  are the linear function parameters. Lastly, We Upsample the Tokens to introduce the lost local features using the association map  $Q$ :

$$\text{Upsample}(\text{Attn}(S)) = Q\text{Attn}(S) \quad (8)$$

| Encoder \ Decoder | No. of layers | Token size | No. of Heads |
|-------------------|---------------|------------|--------------|
| Stage - 1         | 1             | 16 x 16    | 2            |
| Stage - 2         | 2             | 8 x 8      | 4            |
| Stage - 3         | 3             | 4 x 4      | 8            |
| Stage - 4         | 4             | 2 x 2      | 16           |

Table 1. The optimal parameters for Super Token Attention (STA) blocks in the each stage of Encoder/Decoder.

The Multi-head setting is not included for clear understanding. The pseudocode for Super Token Attention can be found in the supplementary material of [15]. The parameter values for the STA blocks for each stage of Encoder and Decoder in UNet are reported in Table 1. We discuss the relationship between performance and choice of parameter values in Section 5.3.

We also visualize the attention maps obtained from the existing transformer-based UNet architectures in Fig. 4. It is worth mentioning that Super Token Attention has precisely given higher weights to the different regions of interest when classifying smaller organs such as Kidneys and Aortas in shallow blocks.

## 4.2. STA-UNet architecture

We dedicate this section to providing a brief overview of the proposed Unet architecture (same is illustrated in Fig 3). Similar to any other UNt architecture, the proposed model comprises Encoder, Decoder, Bottleneck, and Skip connections. The key performance enhancer in this architecture is the Super Token Attention (STA) modules integrated at each stage of the encoder and decoder. On the contrary, with the Transformer Blocks leveraged in the latest UNet architectures [3, 5, 38], we implement dimensional changes in the convolution layers, filtering essential information before applying the attention mechanism. The input image is downsampled to the half dimensions ( $H/2 \times W/2$ ) and channel (C)-dimension is doubled at each stage. The positional embeddings are extracted in the STA Module (in

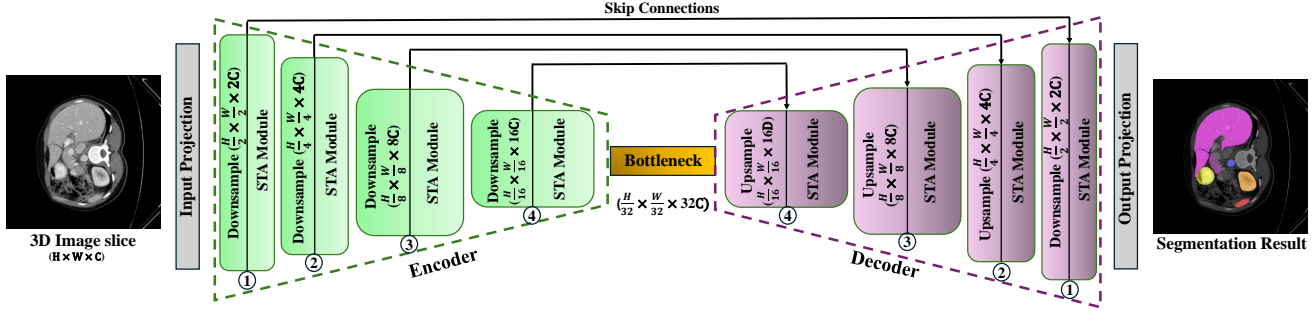


Figure 3. Pictorial representation of the proposed STA-Unet architecture. The number in the circle denote the stage number.

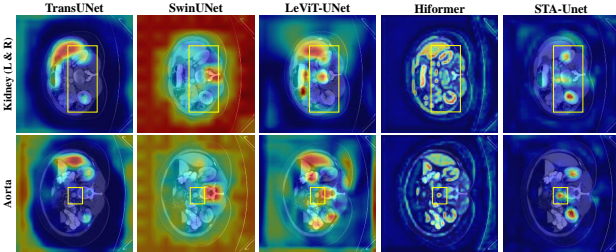


Figure 4. Attention maps from Decoder (Stage-4) Layers for various transformer based UNet architectures.

the CPE stage), followed by Super Tokens generation and calculating the correlation between Tokens and Super Tokens as discussed in Section 4.1. Symmetrical Decoder architecture is adapted with the combination of Upsample block (to obtain the original image shape) and STA modules. The context features extracted during the processing are concatenated with multi-stage features from the encoder through skip connections. This fusion mitigates the loss of spatial information typically incurred by down-sampling, thereby enhancing the model’s ability to retain fine-grained details. Detailed information for each component is documented in this section.

**Encoder** The Encoder consists of two components in each stage. The Downsample block is followed by an STA module. The Downsample block deals with the dimensionality reduction in the forward propagation as we are not relying on the patch merging stage [3]. The Downsampling block is made up of 2 layers of Convolution and Batch Normalization. The convolution layer possesses the kernel size of  $3 \times 3$  and the stride of 2 with padding set to 1. We then process the output features with ReLU [1] activation and reduce the dimensions using the Maxpooling layer. To retain the complete spatial information from this stage, we pass the output from ReLU activation to the decoder through skip connections, unlike the traditional Unet architecture.

**Decoder** Drawing inspiration from [30], the Decoder is designed to be symmetrical to the encoder. Decoder also consists of two components, i.e., the Upsample block and the STA module. Upsample block consists of a ConvTranspose2d layer to increase the spatial dimensions of the in-

put features, followed by the convolution layer similar to the one discussed in Encoder (Section 4.2). We concatenate the feature map from the encoder passed through the skip connection with the features obtained from the previous decoder stage (output from the STA module). The complete spatial information (before Maxpooling in Encoder) helps us present the spatial information along with the contextual features from the attention mechanism for improved learning. We then input the resultant to the Upsample block. The Decoder then passes the output to the Output projection layer to obtain the input image dimensionality and the channel size equal to the segmentation classes. The output is processed through the Softmax layer along the C-axis to obtain the class probabilities.

**Bottleneck** comprises 2 Convolution layers followed by the BatchNorm layer. The ReLU activation function is applied to the output.

## 5. Experiments and results

### 5.1. Datasets

We validated the effectiveness of the proposed method on four publicly available datasets: Synapse Multi-Organ Segmentation, Automated cardiac diagnosis challenge (ACDC) dataset [2], Nuclear segmentation (MoNuSeg) [20, 21], and Gland segmentation in Colon Histology Images (GlaS) [31]. Following [3], [5], [11], we trained the proposed method using the Synapse Multi-Organ Segmentation dataset. The dataset includes 30 cases, encompassing a total of 3,779 axial abdominal CT images. The segmentation masks are provided for 13 abdominal organs, out of which we used 9 classes for training the proposed model. For model development, 18 cases are allocated for training, while 12 cases are designated for testing. Performance is assessed based on the segmentation of eight abdominal organs, with the Average Dice Similarity Coefficient (DSC) used as the primary evaluation metric. The ACDC dataset consists of 100 cardiac MRI scans from a diverse patient cohort, with annotations for the left ventricle (LV), right ventricle (RV), and myocardium (Myo). In line with prior work [5, 29], we partition the dataset into 70 cases (1,930

axial slices) for training, 10 cases for validation, and 20 cases for testing. The performance of our method is evaluated using the Dice Similarity Coefficient (DSC) as the metric. The GlaS [32] and MoNuSeg [22] datasets are the collection of microscopic images. The GlaS dataset contains 85 images designated for training and 80 images for testing. The MoNuSeg dataset includes 30 images for training and 14 images for testing. The performance of the latter two datasets is evaluated using the average Dice Similarity Coefficient (DSC) and Intersection over Union (IoU) as metrics.

### 5.2. Implementation details

We followed the straightforward training regime for easy reproducibility methods [3, 5, 36, 40]. The Synapse CT dataset consists of 3D CT scans with each slice mapped in the Grayscale domain. To train on this dataset, we extracted each slice and center-cropped it to retain the 224 x 224 image for the input. We trained our model for 300 epochs using a Stochastic Gradient Descent (SGD) optimizer for smoother convergence. The batch size was set to 8. The initial learning rate  $lr_{initial}$  was set to be  $1 \times 10^{-2}$ . The learning rate for each iteration  $lr_t$  of the epoch is determined by the Eq. 9. Where  $t$  denotes the current iteration,  $N$  denotes the maximum number of iterations in one epoch.

$$lr_t = lr_{initial} \times \left(1.0 - \frac{t}{N}\right)^{0.9} \quad (9)$$

We trained the model to converge on the summation of Cross-Entropy and Dice loss, maintaining the weights of 0.4 and 0.6, respectively. To tackle the limited dataset problem, we incorporated the following data augmentation traits: Random flips (Horizontal) and rotations with a probability of 0.5. We followed the same experimental setup for the ACDC dataset. For GlaS and MoNuSeg datasets, the batch size was 18. We used the initial learning rate of  $1 \times 10^{-3}$  and updated the learning rate using Cosine Scheduler. We utilized the computational power of Nvidia RTX3090 with 24G memory to conduct our experiments. We compare our methods with recent SOTA models, including UNet [30], R50 U-Net [7], Att-UNet [28], TransUNet [5], SwinUNet [3], LeViT-UNet [38], HiFormer [11], and SegSwinUNet [40].

### 5.3. Ablation Study

Understanding the impact of individual parameters on model performance is crucial for determining the optimal architecture. To gain insights into the effects of varying Token size and Attention heads in our proposed model, we conducted an ablation study on the GlaS dataset.

Table 2. Performance of STA-UNet with different Attention heads at each stage. The  $\rightarrow$  indicates a level change in Encoder, and the reverse trend is followed with the token sizes in Decoder.

| Attention heads<br>(from Stage 1 to 4)               | Mean Dice (%) | IOU (%) |
|--|---------------|---------|
| 8 $\rightarrow$ 16 $\rightarrow$ 32 $\rightarrow$ 64 | 89.91         | 76.95   |
| 4 $\rightarrow$ 8 $\rightarrow$ 16 $\rightarrow$ 32  | 90.41         | 83.27   |
| 2 $\rightarrow$ 4 $\rightarrow$ 8 $\rightarrow$ 16   | 91.03         | 84.29   |
| 1 $\rightarrow$ 2 $\rightarrow$ 4 $\rightarrow$ 8    | 90.56         | 83.52   |

In transformer-based architectures, increasing attention heads often leads the model to capture information from more regions and determine the importance with respect to the decision. It is evident from Table 2 that the super token attention mechanism can achieve superior performance with limited attention heads, bringing down the overlap in focus or redundancy. The same is illustrated in Fig. 5 (a). We chose the highlighted Attention heads trend based on the performance of our proposed method.

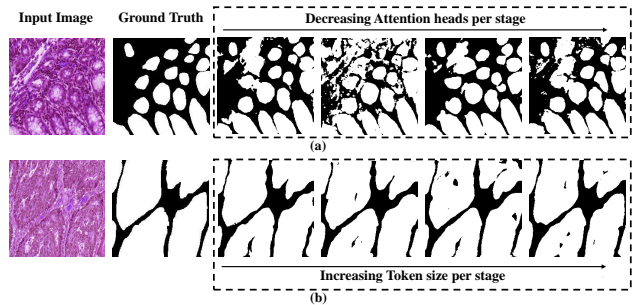


Figure 5. Illustration of Ablation studies on GlaS dataset. (a) Decreasing the attention heads leads to the accurate segmentation of Glands. (b) Increasing the Token size leads to indistinguishable changes.

The Token size impacts the model’s ability to capture spatial details and contextual information. Larger tokens provide broader context but can reduce resolution, while smaller tokens capture finer details but may increase computational complexity. The same is evident from Table 3. Balancing token size is crucial for optimizing both model performance and efficiency.

Table 3. Performance of STA-UNet with different Token sizes at each stage. The  $\rightarrow$  indicates a level change in Encoder, and the reverse trend is followed with the token sizes in Decoder.

| Token size<br>(from Stage 1 to 4)                   | FLOPs                 | Mean Dice | IOU   |
|---|-----------------------|-----------|-------|
| 32 $\rightarrow$ 16 $\rightarrow$ 8 $\rightarrow$ 4 | $59.02 \times 10^3 M$ | 90.8      | 83.80 |
| 16 $\rightarrow$ 8 $\rightarrow$ 4 $\rightarrow$ 2  | $60.30 \times 10^3 M$ | 91.03     | 84.29 |
| 8 $\rightarrow$ 4 $\rightarrow$ 2 $\rightarrow$ 1   | $67.92 \times 10^3 M$ | 90.80     | 83.81 |
| 4 $\rightarrow$ 2 $\rightarrow$ 1 $\rightarrow$ 1   | $91.95 \times 10^3 M$ | 90.31     | 83.76 |

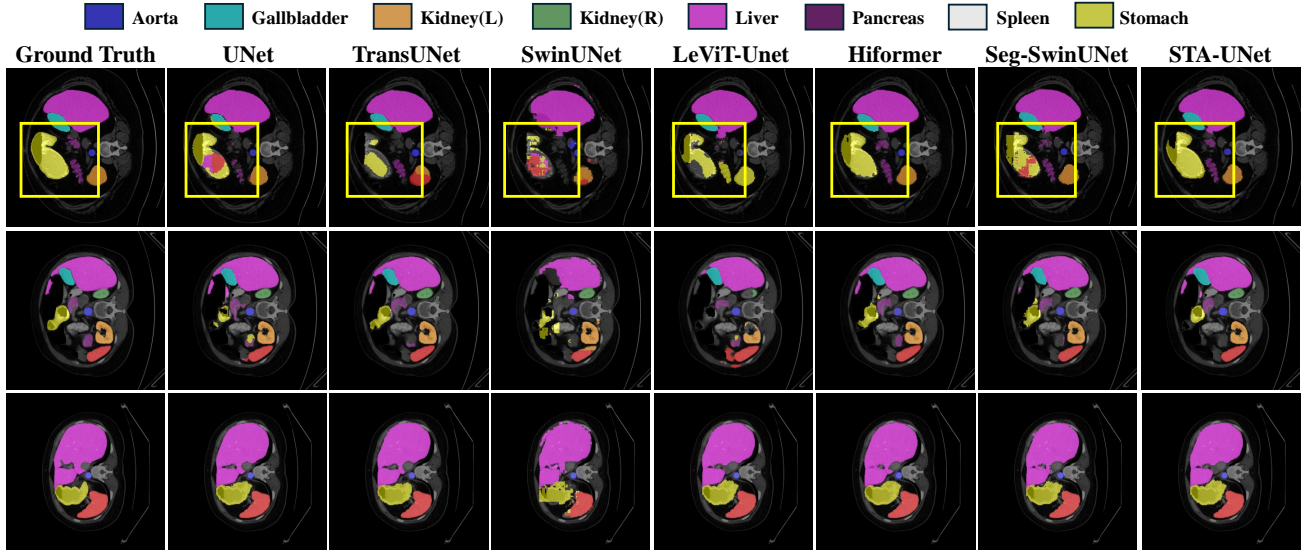


Figure 6. Comparison of segmentation performance in Synapse dataset with Transformer-based UNet architectures. Yellow box highlights how the baseline methods handled Pancreas and Spleen segmentation.

Table 4. Comparison with SOTA methods on Synapse multi-organ CT dataset.  $\Delta_{UNet}$  denotes the improvement gain (%) by comparing with the U-Net [30].  $\Delta_{TransUNet}$  denotes the improvement gain (%) by comparing with the TransUNet [5]

| Methods              | Average DSC  | Aorta | Gallbladder | Kidney(L) | Kidney(R) | Liver | Pancreas | Spleen | Stomach |
|----------------------|--------------|-------|-------------|-----------|-----------|-------|----------|--------|---------|
| R50 U-Net            | 74.68        | 87.74 | 63.66       | 80.60     | 78.19     | 93.74 | 56.90    | 85.87  | 74.16   |
| R50 Att-UNet         | 75.57        | 55.92 | 63.91       | 79.20     | 72.71     | 93.56 | 49.37    | 87.19  | 74.95   |
| Att-UNet             | 77.77        | 89.55 | 68.88       | 77.98     | 71.11     | 93.57 | 58.04    | 87.30  | 75.75   |
| U-Net                | 76.85        | 89.07 | 69.72       | 77.77     | 68.60     | 93.43 | 53.98    | 86.67  | 75.58   |
| TransUNet            | 77.48        | 87.23 | 63.13       | 81.87     | 77.02     | 94.08 | 55.86    | 85.08  | 75.62   |
| SwinUNet             | 79.13        | 85.47 | 66.53       | 83.28     | 79.61     | 94.29 | 56.58    | 90.66  | 76.60   |
| LeViT-UNet           | 78.53        | 78.53 | 62.23       | 84.61     | 80.25     | 93.11 | 59.07    | 88.86  | 72.76   |
| HiFormer             | 80.29        | 85.63 | 73.29       | 82.39     | 64.84     | 94.22 | 60.84    | 91.03  | 78.07   |
| Seg-SwinUNet         | 80.54        | 86.07 | 69.65       | 85.12     | 82.58     | 94.18 | 61.08    | 87.42  | 78.22   |
| STA-UNet             | <b>80.69</b> | 89.10 | 68.34       | 84.97     | 79.44     | 93.39 | 63.32    | 88.69  | 78.26   |
| $\Delta_{UNet}$      | +4.99        | +3.00 | -1.97       | +9.25     | +15.80    | -0.43 | +17.30   | +2.33  | +3.54   |
| $\Delta_{TransUNet}$ | +4.14        | +2.14 | +8.25       | +3.70     | +3.10     | -0.73 | +13.35   | +4.24  | +3.49   |

But in the proposed Super Token Attention approach, we notice that the performance has very minute changes with the change of token size, Thus limiting the dependency of performance over the Token size; the same is evident from Fig. 5 (b). Based on the study, we chose the model with relatively lower Floating Point Operations per second to lower the computational complexity.

#### 5.4. Results

The performance analysis is reported in Table 4 for the Synapse dataset, Table 5 for the ACDC dataset, and Table 6 for Glas and MoNuSeg datasets. Our main conclusion is that our proposed architecture is effective and computationally rational and achieved significant improvement over quantitative metrics. We reported the gain/loss in percent

with respect to the UNet [30] and the first-ever proposed transformer-based UNet architecture, TransUNet [5]. We observe substantial improvements of 4.99%, 2.86%, 6.53%, and 6.03% across the four datasets when compared to UNet. Similarly, compared to TransUNet, our approach demonstrates gains of 4.14%, 2.83%, 2.97%, and 3.22%, respectively. When compared with recently established works like HiFormer [11] and Seg-Swinunet [40], we achieved 0.49% and 0.18% DSC improvement, respectively. This huge gain in DSC resulted from segmenting the difficult organs such as the Kidneys (L&R) and Pancreas more accurately. The same is illustrated from Fig 6. We throw the light on Pancreas and Stomach segmentation highlighted in the Yellow (First row in Fig. 6). Notably, SwinUNet could not segment either of them and other models [5, 38, 40] have not

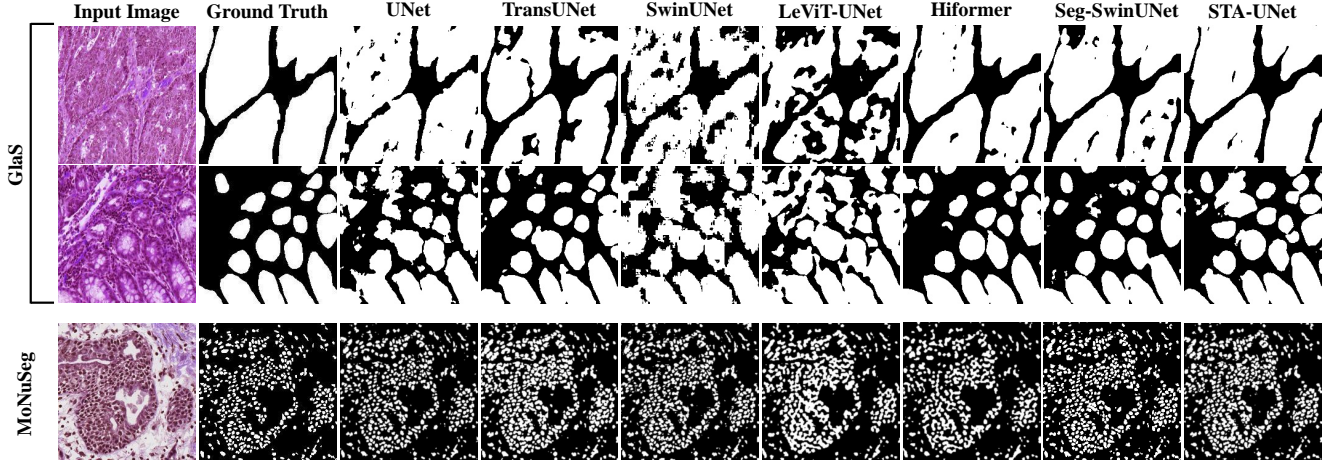


Figure 7. Comparison of segmentation performance on Glas (Glands) and MoNuSeg (Nuclear) Dataset.

completely segmented the pancreas. The proposed model tackled this challenge very well and was on par with HiFormer.

Table 5. Comparison of different methods in ACDC dataset.  $\Delta_{UNet}$  denotes the improvement gain (%) by comparing with the U-Net.  $\Delta_{TransUNet}$  denotes the improvement gain (%) by comparing with the TransUNet.

| Methods              | Avg DSC      | RV    | Myo   | LV    |
|----------------------|--------------|-------|-------|-------|
| UNet                 | 89.68        | 87.17 | 87.21 | 94.68 |
| TransUNet            | 89.71        | 86.67 | 87.27 | 95.18 |
| SwinUNet             | 88.07        | 85.77 | 84.42 | 94.03 |
| LeViT-UNet           | 88.21        | 85.56 | 84.75 | 94.32 |
| Hiformer             | 90.82        | 88.55 | 88.44 | 95.47 |
| Seg-SwinUNet         | 91.49        | 89.49 | 89.27 | 95.70 |
| STA-Unet             | <b>92.25</b> | 90.31 | 90.44 | 95.99 |
| $\Delta_{UNet}$      | +2.86        | +3.60 | +2.36 | +1.38 |
| $\Delta_{TransUNet}$ | +2.83        | +4.19 | +3.63 | +0.85 |

We established the Generalizability of our work by improving the DSC by 2.86%, 6.53%, and 6.03% on ACDC, Glas, and MoNuSeg datasets, respectively, compared with UNet. We also outperformed all the Transformer based UNet architectures for segmentation tasks on ACDC and MoNuSeg and stood second best with a very minute difference of 0.64% in DSC for Glas dataset (refer to Table. 5 & 6). We visually compared the performance of Gland (using Glas) and Nuclear (using MoNuSeg) Segmentation in Fig. 7. Poor foreground classification for Gland segmentation is clearly visible from the predictions of SwinUNet and LeViT-UNet (the top two rows in Fig 7), which has been remarkably tackled by the proposed Super Token Attention (STA-UNet) yielding accurate segmentation. We also highlight the difficulty distinguishing the foreground and background in the Glas dataset. In the case of MoNuSeg, our

Table 6. Comparison of different methods in Glas and MoNuSeg datasets. The second best performance is underlined.

| Method               | Glas              |                   | MoNuSeg           |                   |
|----------------------|-------------------|-------------------|-------------------|-------------------|
|                      | DSC (%)           | IOU (%)           | DSC (%)           | IOU (%)           |
| UNet                 | 85.45±1.25        | 74.78±1.67        | 76.45±2.62        | 62.86±3.00        |
| TransUNet            | 88.40±0.74        | 80.40±1.04        | 78.53±1.06        | 65.05±1.28        |
| SwinUNet             | 89.58±0.57        | 82.06±0.73        | 77.69±0.94        | 63.77±1.15        |
| LeViT-UNet           | 81.19±1.38        | 69.73±1.85        | 70.28±3.92        | 53.08±0.43        |
| Hiformer             | 90.97±0.23        | 83.99±0.44        | 72.51±0.87        | 57.03±0.98        |
| Seg-SwinUNet         | <b>91.62±0.16</b> | <b>85.29±0.30</b> | 79.38±0.15        | 65.87±0.21        |
| STA-Unet             | 91.03±0.58        | 84.29±0.94        | <b>81.06±0.66</b> | <b>68.24±0.80</b> |
| $\Delta_{UNet}$      | +6.53             | +12.71            | +6.03             | +8.55             |
| $\Delta_{TransUNet}$ | +2.97             | +4.84             | +3.22             | +4.90             |

proposed model achieves results that are highly comparable to the ground truth, capturing complete shapes and maintaining clear backgrounds, even in challenging samples (as shown in the third row of Fig. 7). These findings reinforce our assertion that STA-UNet enhances segmentation performance, even with the reduced redundancy in shallow layer features typically seen in Transformer-based architectures.

## 6. Conclusion

In this study, we re-introduce Super Token Attention (STA) in UNet architecture as an STA Module to tackle the feature redundancy inherently present in existing transformer-based architectures while enhancing performance over organ segmentation tasks. We reported the preliminary analysis to mathematically make the redundancy present in Transformer-based architectures evident and encourage the research to mitigate the same. Our findings demonstrated a notable improvement over existing benchmarks across four publicly available datasets, evidencing the potential of STA-UNet in Medical Image Segmentation. Our extensive ablation study explains the impact on perfor-

mance caused by two major parameter changes, i.e., Token size and Number of Attention heads. While our experiments are limited to the multi-organ segmentation tasks, the STA-UNet has the potential for broader applications such as Anomaly detection and restoration in various medical datasets. We anticipate further exploring the utility of the proposed architecture in other medical image applications in future research.

## References

- [1] Abien Fred Agarap. Deep learning using rectified linear units (relu), 2019. [5](#)
- [2] Olivier Bernard, Alain Lalonde, Clement Zotti, Frederick Cervenansky, Xin Yang, Pheng-Ann Heng, Irem Cetin, Karim Lekadir, Oscar Camara, Miguel Angel Gonzalez Ballester, Gerard Sanroma, Sandy Napel, Steffen Petersen, Georgios Tziritas, Elias Grinias, Mahendra Khened, Varghese Alex Kollerathu, Ganapathy Krishnamurthi, Marc-Michel Rohé, Xavier Pennec, Maxime Sermesant, Fabian Isensee, Paul Jäger, Klaus H. Maier-Hein, Peter M. Full, Ivo Wolf, Sandy Engelhardt, Christian F. Baumgartner, Lisa M. Koch, Jelmer M. Wolterink, Ivana Išgum, Yeonggul Jang, Yoonmi Hong, Jay Patravali, Shubham Jain, Olivier Humbert, and Pierre-Marc Jodoin. Deep learning techniques for automatic mri cardiac multi-structures segmentation and diagnosis: Is the problem solved? *IEEE Transactions on Medical Imaging*, 37(11):2514–2525, 2018. [5](#)
- [3] Hu Cao, Yueyue Wang, Joy Chen, Dongsheng Jiang, Xiaopeng Zhang, Qi Tian, and Manning Wang. Swin-UNET: Unet-like pure transformer for medical image segmentation, 2021. [2](#), [4](#), [5](#), [6](#)
- [4] Nicolas Carion, Francisco Massa, Gabriel Synnaeve, Nicolas Usunier, Alexander Kirillov, and Sergey Zagoruyko. End-to-end object detection with transformers, 2020. [1](#)
- [5] Jieneng Chen, Yongyi Lu, Qihang Yu, Xiangde Luo, Ehsan Adeli, Yan Wang, Le Lu, Alan L. Yuille, and Yuyin Zhou. TransUNet: Transformers make strong encoders for medical image segmentation, 2021. [1](#), [2](#), [4](#), [5](#), [6](#), [7](#)
- [6] Fahim Dalvi, Hassan Sajjad, Nadir Durrani, and Yonatan Belinkov. Analyzing redundancy in pretrained transformer models, 2020. [2](#)
- [7] Foivos I. Diakogiannis, François Waldner, Peter Caccetta, and Chen Wu. ResUNet-a: A deep learning framework for semantic segmentation of remotely sensed data. *ISPRS Journal of Photogrammetry and Remote Sensing*, 162:94–114, apr 2020. [6](#)
- [8] Alexey Dosovitskiy, Lucas Beyer, Alexander Kolesnikov, Dirk Weissenborn, Xiaohua Zhai, Thomas Unterthiner, Mostafa Dehghani, Matthias Minderer, Georg Heigold, Sylvain Gelly, Jakob Uszkoreit, and Neil Houlsby. An image is worth 16x16 words: Transformers for image recognition at scale, 2021. [1](#), [2](#)
- [9] Ben Graham, Alaaeldin El-Nouby, Hugo Touvron, Pierre Stock, Armand Joulin, Hervé Jégou, and Matthijs Douze. Levit: a vision transformer in convnet’s clothing for faster inference, 2021. [2](#)
- [10] Ali Hatamizadeh, Yucheng Tang, Vishwesh Nath, Dong Yang, Andriy Myronenko, Bennett Landman, Holger Roth, and Daguang Xu. UNETR: Transformers for 3d medical image segmentation, 2021. [1](#)
- [11] Moein Heidari, Amirhossein Kazerouni, Milad Soltany, Reza Azad, Ehsan Khodapanah Aghdam, Julien Cohen-Adad, and Dorit Merhof. Hiformer: Hierarchical multi-scale representations using transformers for medical image segmentation, 2023. [2](#), [3](#), [5](#), [6](#), [7](#)
- [12] K. Held, E.R. Kops, B.J. Krause, W.M. Wells, R. Kikinis, and H.-W. Muller-Gartner. Markov random field segmentation of brain mr images. *IEEE Transactions on Medical Imaging*, 16(6):878–886, Dec. 1997. [2](#)
- [13] Dan Hendrycks and Kevin Gimpel. Gaussian error linear units (gelus), 2023. [4](#)
- [14] Huimin Huang, Lanfen Lin, Ruofeng Tong, Hongjie Hu, Qiaowei Zhang, Yutaro Iwamoto, Xianhua Han, Yen-Wei Chen, and Jian Wu. Unet 3+: A full-scale connected unet for medical image segmentation, 2020. [2](#)
- [15] Huaibo Huang, Xiaoqiang Zhou, Jie Cao, Ran He, and Tieniu Tan. Vision transformer with super token sampling, 2024. [2](#), [3](#), [4](#)
- [16] Fabian Isensee, Paul F Jaeger, Simon AA Kohl, Jens Petersen, and Klaus H Maier-Hein. nnu-net: a self-configuring method for deep learning-based biomedical image segmentation. *Nature methods*, 18(2):203–211, 2021. [1](#)
- [17] Varun Jampani, Deqing Sun, Ming-Yu Liu, Ming-Hsuan Yang, and Jan Kautz. Superpixel sampling networks, 2018. [3](#), [4](#)
- [18] Qiangguo Jin, Zhaopeng Meng, Changming Sun, Hui Cui, and Ran Su. Ra-unet: A hybrid deep attention-aware network to extract liver and tumor in ct scans. *Frontiers in Bioengineering and Biotechnology*, 8, Dec. 2020. [1](#)
- [19] Simon Kornblith, Mohammad Norouzi, Honglak Lee, and Geoffrey Hinton. Similarity of neural network representations revisited. In *International conference on machine learning*, pages 3519–3529. PMLR, 2019. [3](#)
- [20] Neeraj Kumar, Ruchika Verma, Deepak Anand, Yanning Zhou, Omer Fahri Onder, Efstratios Tsougenis, Hao Chen, Pheng-Ann Heng, Jiahui Li, Zhiqiang Hu, Yunzhi Wang, Navid Alemi Koochbanani, Mostafa Jahanifar, Neda Zamani Tajeddin, Ali Gooya, Nasir Rajpoot, Xuhua Ren, Sihang Zhou, Qian Wang, Dinggang Shen, Cheng-Kun Yang, Chi-Hung Weng, Wei-Hsiang Yu, Chao-Yuan Yeh, Shuang Yang, Shuoyu Xu, Pak Hei Yeung, Peng Sun, Amirreza Mahbod, Gerald Schaefer, Isabella Ellinger, Rupert Ecker, Orjan Smedby, Chunliang Wang, Benjamin Chidester, That-Vinh Ton, Minh-Triet Tran, Jian Ma, Minh N. Do, Simon Graham, Quoc Dang Vu, Jin Tae Kwak, Akshaykumar Gunda, Raviteja Chunduri, Corey Hu, Xiaoyang Zhou, Dariush Lotfi, Reza Safdari, Antanas Kascenas, Alison O’Neil, Dennis Eschweiler, Johannes Stegmaier, Yanping Cui, Baocai Yin, Kailin Chen, Xinmei Tian, Philipp Gruening, Erhardt Barth, Elad Arbel, Itay Remer, Amir Ben-Dor, Ekaterina Sirazitdinova, Matthias Kohl, Stefan Braunewell, Yuexiang Li, Xinpeng Xie, Linlin Shen, Jun Ma, Krishanu Das Baksi, Mohammad Azam Khan, Jaegul Choo, Adrián Colomer, Valery Naranjo, Linmin Pei, Khan M. Iftekharruddin, Kaushiki Roy, Debotosh Bhattacharjee, Anibal Pedraza, Maria Gloria Bueno, Sabarinathan Devanathan, Saravanan Radhakrishnan, Praveen Koduganty, Zihan Wu, Guanyu Cai, Xiaojie Liu, Yuqin Wang, and Amit Sethi. A multi-organ nucleus segmentation challenge. *IEEE Transactions on Medical Imaging*, 39(5):1380–1391, 2020. [5](#)
- [21] Neeraj Kumar, Ruchika Verma, Sanuj Sharma, Surabhi Bhargava, Abhishek Vahadane, and Amit Sethi. A dataset and a technique for generalized nuclear segmentation for

- computational pathology. *IEEE transactions on medical imaging*, 36(7):1550–1560, 2017. 5
- [22] Neeraj Kumar, Ruchika Verma, Sanuj Sharma, Surabhi Bhargava, Abhishek Vahadane, and Amit Sethi. A dataset and a technique for generalized nuclear segmentation for computational pathology. *IEEE Transactions on Medical Imaging*, 36(7):1550–1560, 2017. 6
- [23] Hao Li, Asim Kadav, Igor Durdanovic, Hanan Samet, and Hans Peter Graf. Pruning filters for efficient convnets, 2017. 2
- [24] Lujun Li. Self-regulated feature learning via teacher-free feature distillation. In *European Conference on Computer Vision*, pages 347–363. Springer, 2022. 2
- [25] Xiaomeng Li, Hao Chen, Xiaojuan Qi, Qi Dou, Chi-Wing Fu, and Pheng Ann Heng. H-denseunet: Hybrid densely connected unet for liver and tumor segmentation from ct volumes, 2018. 2
- [26] Yanghao Li, Chao-Yuan Wu, Haoqi Fan, Karttikeya Mangalam, Bo Xiong, Jitendra Malik, and Christoph Feichtenhofer. Mvitv2: Improved multiscale vision transformers for classification and detection, 2022. 4
- [27] Ze Liu, Yutong Lin, Yue Cao, Han Hu, Yixuan Wei, Zheng Zhang, Stephen Lin, and Baining Guo. Swin transformer: Hierarchical vision transformer using shifted windows, 2021. 1, 2, 4
- [28] Ozan Oktay, Jo Schlemper, Loic Le Folgoc, Matthew Lee, Mattias Heinrich, Kazunari Misawa, Kensaku Mori, Steven McDonagh, Nils Y Hammerla, Bernhard Kainz, et al. Attention u-net: Learning where to look for the pancreas. *arXiv preprint arXiv:1804.03999*, 2018. 2, 3, 6
- [29] Md Mostafijur Rahman and Radu Marculescu. Medical image segmentation via cascaded attention decoding. In *2023 IEEE/CVF Winter Conference on Applications of Computer Vision (WACV)*, pages 6211–6220, 2023. 5
- [30] Olaf Ronneberger, Philipp Fischer, and Thomas Brox. U-net: Convolutional networks for biomedical image segmentation, 2015. 1, 2, 5, 6, 7
- [31] Korsuk Sirinukunwattana, Josien P. W. Pluim, Hao Chen, Xiaojuan Qi, Pheng-Ann Heng, Yun Bo Guo, Li Yang Wang, Bogdan J. Matuszewski, Elia Bruni, Urko Sanchez, Anton Böhm, Olaf Ronneberger, Bassem Ben Cheikh, Daniel Racoceanu, Philipp Kainz, Michael Pfeiffer, Martin Urschler, David R. J. Snead, and Nasir M. Rajpoot. Gland segmentation in colon histology images: The glas challenge contest, 2016. 5
- [32] Korsuk Sirinukunwattana, Josien P. W. Pluim, Hao Chen, Xiaojuan Qi, Pheng-Ann Heng, Yun Bo Guo, Li Yang Wang, Bogdan J. Matuszewski, Elia Bruni, Urko Sanchez, Anton Böhm, Olaf Ronneberger, Bassem Ben Cheikh, Daniel Racoceanu, Philipp Kainz, Michael Pfeiffer, Martin Urschler, David R. J. Snead, and Nasir M. Rajpoot. Gland segmentation in colon histology images: The glas challenge contest, 2016. 6
- [33] A. Tsai, A. Yezzi, W. Wells, C. Tempny, D. Tucker, A. Fan, W.E. Grimson, and A. Willsky. A shape-based approach to the segmentation of medical imagery using level sets. *IEEE Transactions on Medical Imaging*, 22(2):137–154, 2003. 2
- [34] Ashish Vaswani, Noam Shazeer, Niki Parmar, Jakob Uszkoreit, Llion Jones, Aidan N. Gomez, Lukasz Kaiser, and Illia Polosukhin. Attention is all you need, 2023. 1, 2, 4
- [35] Haonan Wang, Peng Cao, Jiaqi Wang, and Osmar R. Zaiane. Uctransnet: Rethinking the skip connections in u-net from a channel-wise perspective with transformer, 2022. 2, 3
- [36] Haonan Wang, Peng Cao, Jiaqi Wang, and Osmar R Zaiane. Uctransnet: rethinking the skip connections in u-net from a channel-wise perspective with transformer. In *Proceedings of the AAAI conference on artificial intelligence*, volume 36, pages 2441–2449, 2022. 6
- [37] Xiao Xiao, Shen Lian, Zhiming Luo, and Shaozi Li. Weighted res-unet for high-quality retina vessel segmentation. In *2018 9th International Conference on Information Technology in Medicine and Education (ITME)*, pages 327–331, 2018. 2
- [38] Guoping Xu, Xuan Zhang, Xinwei He, and Xinglong Wu. Levit-unet: Make faster encoders with transformer for medical image segmentation. In *Chinese Conference on Pattern Recognition and Computer Vision (PRCV)*, pages 42–53. Springer, 2023. 2, 4, 6, 7
- [39] Zongwei Zhou, Md Mahfuzur Rahman Siddiquee, Nima Tajbakhsh, and Jianming Liang. Unet++: A nested u-net architecture for medical image segmentation, 2018. 2, 3
- [40] Wenhui Zhu, Xiwen Chen, Peijie Qiu, Mohammad Farazi, Aristeidis Sotiras, Abolfazl Razi, and Yalin Wang. Selfreg-unet: Self-regularized unet for medical image segmentation, 2024. 2, 3, 6, 7